Supplementary information

Materials and Methods

Constructs of 5-HT_{1F} and G_{i1} heterotrimer

The full-length gene sequences of wild-type human 5-HT_{1F} receptors were subcloned into pFastbac vector using ClonExpress II One Step Cloning Kit (Vazyme Biotech Co.,Ltd). An N-terminal thermally stabilized BRIL[1] as a fusion protein to enhance receptor expression. N-terminal fusions of Flag tag and 8× His tag were used to facilitate protein purification. A dominant-negative $G\alpha_{i1}$ was generated by site-directed mutagenesis to incorporate mutations S47N, G203A, A326S, and E245A that improves the dominant-negative effect by weakening a salt bridge that helps to stabilize the interactions with the βγ subunits[2]. All the three G_i subunits, human DN_$G\alpha_{i1}$, wild-type Gβ1, and Gγ2 were cloned into the pFastBac vector separately. A no-tag single-chain antibody scFv16[3] was cloned into pFastBac.

Insect cell expression

Human 5-HT_{1F}, DN$G\alpha_{i1}$, $G\beta_1$, $G\gamma_2$,and scFv16 were co-expressed in *Trichoplusia ni* Hi5 insect cells using the baculovirus method (Expression Systems). Cell cultures were grown in ESF 921 serum-free medium (Expression Systems) to a density of 2–3 million cells per mL and then infected with four separate baculoviruses at a suitable ratio. The culture was collected by centrifugation 48 h after infection and cell pellets were stored at –80 °C.

Complex purification

The complex was purified as previously described[4]. In brief, cell pellets were thawed in 20 mM HEPES, pH 7.4, 50 mM NaCl, 10 mM $MgCl_2$ supplemented with Protease Inhibitor Cocktail (Bimake). The 5-HT_{1F} complex formation was initiated by addition of 10 μM lasmiditan (TargetMol), apyrase (25 mU/mL, Sigma). The suspension was incubated for 1 h at room temperature and the complex was solubilized from the membrane using 0.5% (w/v) n-dodecyl-β-d-maltoside (DDM, Anatrace) and 0.1% (w/v) cholesteryl hemisuccinate (CHS, Anatrace) for 2 h at 4 °C. Insoluble material was removed by

centrifugation at 65,000× *g* for 30 min and the solubilized complex was immobilized by batch binding to Talon affinity resin. The resin was then packed and washed with 20 column volumes of 20 mM HEPES, pH 7.4, 100 mM NaCl, 5 mM $MgCl_2$, 0.01% (w/v) LMNG, and 0.002% (w/v) CHS, 10 μM lasmiditan. Finally, the complex was eluted in buffer containing 300 mM imidazole and concentrated with an Amicon Ultra Centrifugal Filter (MWCO 100 kDa). Complex was subjected to size-exclusion chromatography on a Superdex 200 Increase 10/300 column (GE Healthcare) pre-equilibrated with 20 mM HEPES, pH 7.4, 100 mM NaCl, 0.05% (w/v) digitonin, and 10 μM lasmiditan, to separate complex from contaminants. Eluted fractions consisting of receptor and G_i-protein complex were pooled and concentrated.

NanoBiT G protein recruitment assay

Analysis of G protein recruitment was performed by using a modified protocol of NanoBiT system (Promega) assay described previously[5]. Receptor-LgBiT, $G\alpha_{i1}$, SmBiT-fused $G\beta_1$, and $G\gamma_2$ were co-expressed in *Trichoplusia ni* Hi5 insect cells using the baculovirus method (Expression Systems). Cell cultures were grown in ESF 921 serum-free medium (Expression Systems) to a density of 2–3 million cells per ml and then infected with four separate baculoviruses at a suitable ratio. The culture was collected by centrifugation 48 h after infection and cell pellets were collected with PBS. The cell suspension was dispensed in a white 384-well plate at a volume of 40 μL per well and loaded with 5 μL of 90 μM coelenterazine diluted in the assay buffer. Test compounds (5 μL) were added and incubated for 3–5 min at room temperature before measurement. Luminescence counts were normalized to the initial count and fold-change signals over vehicle treatment were used to show G protein binding response.

Cryo-EM grid preparation and data collection

For the preparation of cryo-EM grids, 3 μL of the purified lasmiditan–5-HT_{1F}–G_i complex at concentration of ~15 mg/mL were applied onto a glow-discharged holey carbon grid (Quantifoil R1.2/1.3 Au 300). Grids were plunge-frozen in liquid ethane using Vitrobot Mark IV (Thermo Fisher

Scientific). Frozen grids were transferred to liquid nitrogen and stored for data acquisition. Cryo-EM imaging was performed on a Titan Krios at 300 kV using Gatan K3 Summit detector in the Cryo-Electron Microscopy Research Center, Shanghai Institute of Materia Medica, Chinese Academy of Sciences (Shanghai, China). The images were recorded at a dose rate of about 26.7 $e^-/Å^2/s$ with a defocus ranging from –1.2 to –2.2 μm. The total exposure time was 3 s and intermediate frames were recorded in 0.083 s intervals, resulting in a total of 36 frames per micrograph.

Image processing and map construction

Dose-fractionated image stacks were aligned using MotionCor2.1[6]. Contrast transfer function (CTF) parameters for each micrograph were estimated by Gctf[7]. Cryo-EM data processing was performed using RELION-3.1[8]. Automated particle picking yielded 4,075,443 particles that were subjected to reference-free 2D classification to discard poorly defined particles, producing 1,467,387 particles. The map of 5-HT_{1B}–miniG_o complex (EMDB-4358)[9] low-pass filtered to 60 Å was used as an initial reference model for 3 rounds of 3D classification. Two subsets show the high-quality receptor density was selected, producing 263,350 particles. The selected subsets was subsequently subjected to 3D refinement, CTF refinement, Bayesian polishing, and DeepEMhancer[10]. The final refinement generated a map with an indicated global resolution of 3.4 Å at a Fourier shell correlation of 0.143. Local resolution was determined using the 3DFSC package with half maps as input maps.

Model building and refinement

The cryo-EM structure of 5-HT_{1B}–mG_o complex (PDB code: 6G79) and the G_i protein model (PDB code: 6PT0) were used as the start for model rebuilding and refinement against the electron microscopy map. The model was docked into the electron microscopy density map using Chimera[11], followed by iterative manual adjustment and rebuilding in COOT[12] and ISOLDE[13]. Real space and reciprocal space refinements were performed using Phenix programs[14]. The model statistics were validated using MolProbity[15]. Structural figures were prepared in Chimerax[16].

References

1 Chun, E. *et al.* Fusion partner toolchest for the stabilization and crystallization of G protein-coupled receptors. *Structure* **20**, 967-976, doi:10.1016/j.str.2012.04.010 (2012).

2 Liang, Y. L. *et al.* Dominant Negative G Proteins Enhance Formation and Purification of Agonist-GPCR-G Protein Complexes for Structure Determination. *ACS Pharmacol Transl Sci* **1**, 12-20, doi:10.1021/acsptsci.8b00017 (2018).

3 Maeda, S. *et al.* Development of an antibody fragment that stabilizes GPCR/G-protein complexes. *Nature Communications* **9**, 3712 (2018).

4 Zhuang, Y. *et al.* Structural insights into the human D1 and D2 dopamine receptor signaling complexes. *Cell* **184**, 931-942 (2021).

5 Xu, P. *et al.* Structures of the human dopamine D3 receptor-Gi complexes. *Mol. Cell* **81**, 1147-1159 (2021).

6 Zheng, S. Q. *et al.* MotionCor2: anisotropic correction of beam-induced motion for improved cryo-electron microscopy. *Nat Methods* **14**, 331-332, doi:10.1038/nmeth.4193 (2017).

7 Zhang, K. Gctf: Real-time CTF determination and correction. *J Struct Biol* **193**, 1-12, doi:10.1016/j.jsb.2015.11.003 (2016).

8 Scheres, S. H. W. RELION: Implementation of a Bayesian approach to cryo-EM structure determination. *J Struct Biol* **180**, 519-530, doi:10.1016/j.jsb.2012.09.006 (2012).

9 Kato, H. E. *et al.* Conformational transitions of a neurotensin receptor 1-Gi1 complex. *Nature* **572**, 80-85, doi:10.1038/s41586-019-1337-6 (2019).

10 Sanchez-Garcia, R. *et al.* DeepEMhancer: a deep learning solution for cryo-EM volume post-processing. *bioRxiv* https://doi.org/10.1101/2020.06.12.148296 (2020).

11 Pettersen, E. F. *et al.* UCSF Chimera--a visualization system for exploratory research and analysis. *J Comput Chem* **25**, 1605-1612, doi:10.1002/jcc.20084 (2004).

12 Emsley, P. & Cowtan, K. Coot: model-building tools for molecular graphics. *Acta Crystallogr D Biol Crystallogr* **60**, 2126-2132, doi:10.1107/S0907444904019158 (2004).

13 Croll, T. I. ISOLDE: a physically realistic environment for model building into low-resolution electron-density maps. *Acta Crystallogr D Struct Biol* **74**, 519-530, doi:10.1107/S2059798318002425 (2018).

14 Adams, P. D. *et al.* PHENIX: a comprehensive Python-based system for macromolecular structure solution. *Acta Crystallogr D Biol Crystallogr* **66**, 213-221, doi:10.1107/S0907444909052925 (2010).

15 Chen, V. B. *et al.* MolProbity: all-atom structure validation for macromolecular crystallography. *Acta Crystallogr D* **66**, 12-21, doi:10.1107/S0907444909042073 (2010).

16 Pettersen, E. F. *et al.* UCSF ChimeraX: Structure visualization for researchers, educators, and developers. *Protein Sci*, **30**, 70-82, doi:10.1002/pro.3943 (2021).

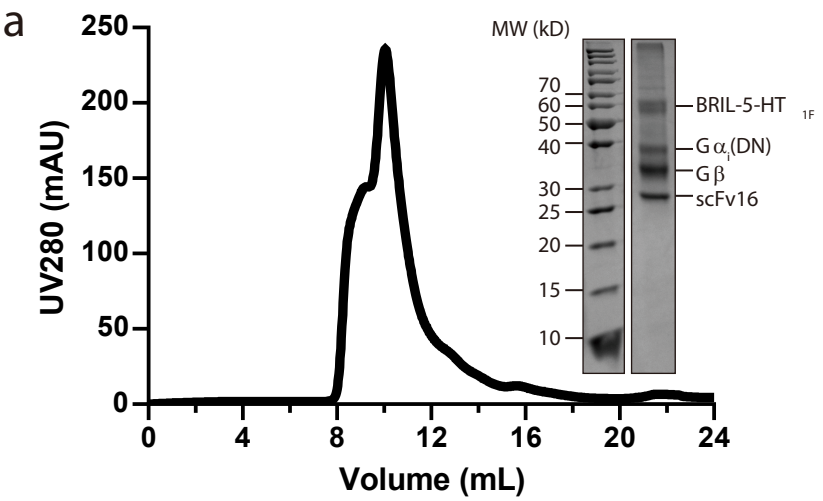
a
UV280 (mAU)
Volume (mL)
MW (kD)
BRIL-5-HT 1F
Gαi(DN)
Gβ
scFv16

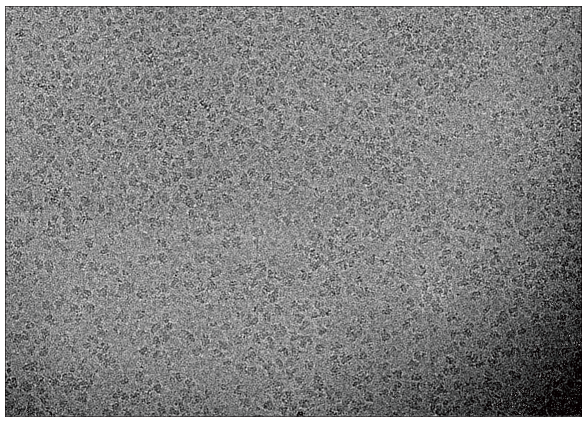
b

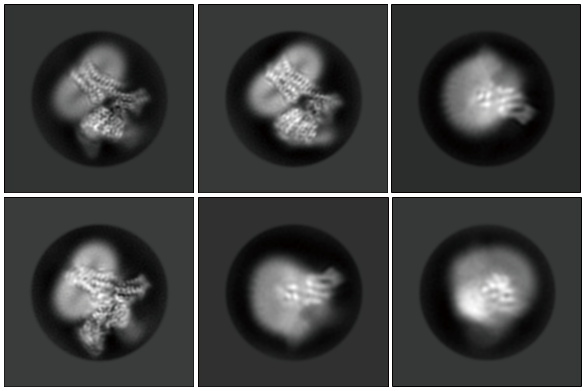
c

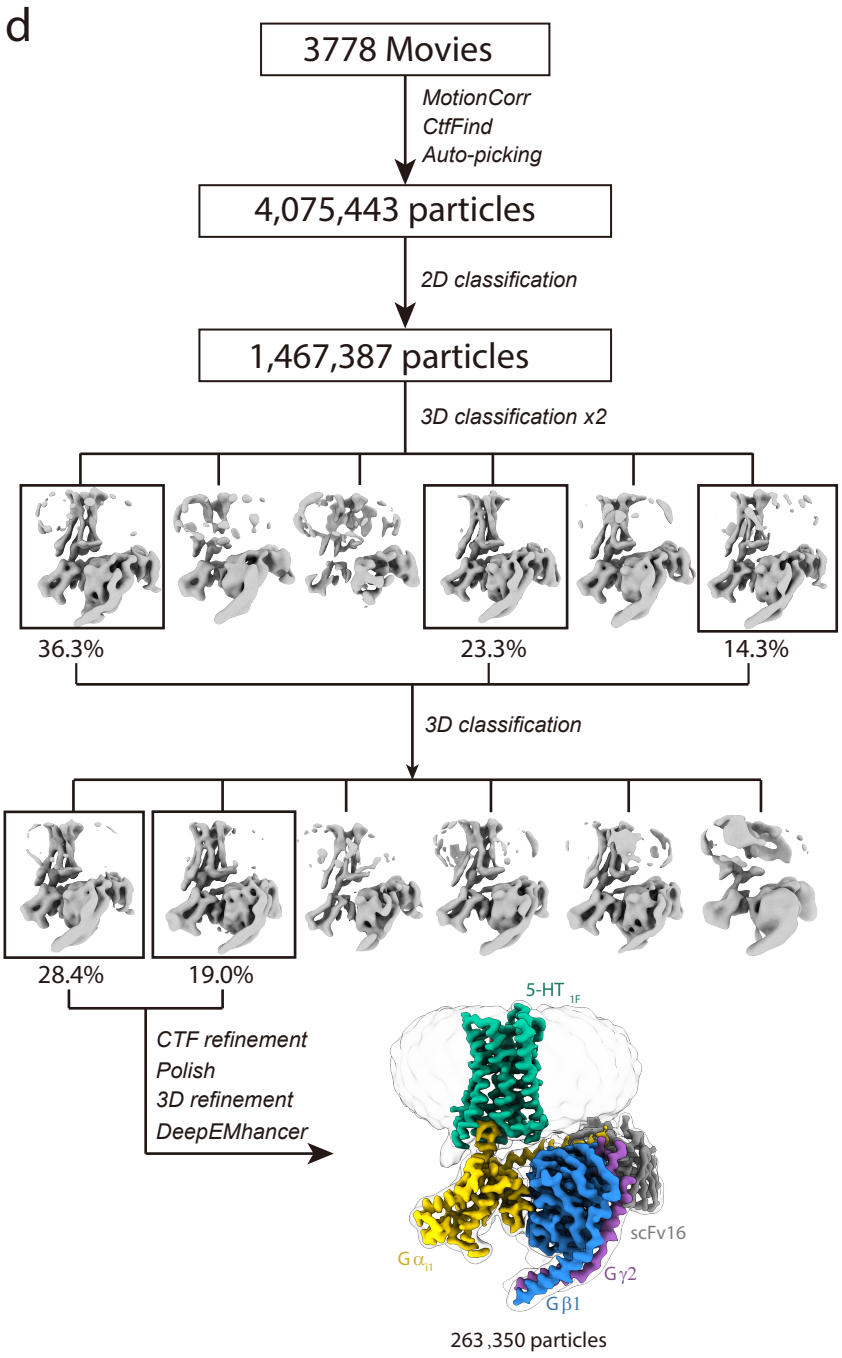
d
3778 Movies
MotionCorr
CtfFind
Auto-picking
4,075,443 particles
2D classification
1,467,387 particles
3D classification x2
36.3%
23.3%
14.3%
3D classification
28.4%
19.0%
CTF refinement
Polish
3D refinement
DeepEMhancer
5-HT 1F
scFv16
Gγ2
Gβ1
263,350 particles

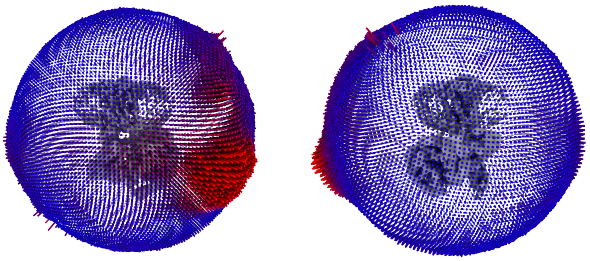
e

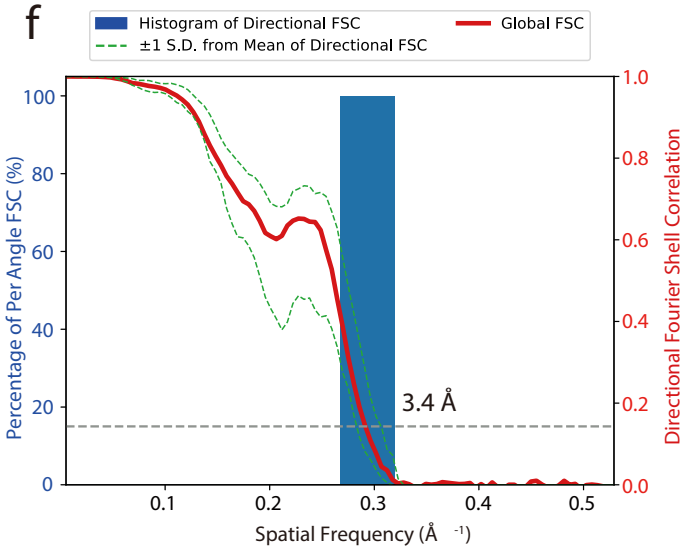
f
Histogram of Directional FSC
Global FSC
±1 S.D. from Mean of Directional FSC
Percentage of Per Angle FSC (%)
Directional Fourier Shell Correlation
3.4 Å
Spatial Frequency (Å -1)

Supplementary information, Fig. S1 Sample preparation and cryo-EM of the 5-HT_{1F}–G_{i1} complexes. a Analytical size-exclusion chromatography of the purified complex and SDS-PAGE/Coomassie blue stain of the purified complex. **b**, **c** Representative cryo-EM image and 2D averages. **d** Flowchart of cryo-EM data analysis of the lasmiditan-bound 5-HT_{1F}–G_i complex. **e** Euler angle distribution of particles used in the final reconstruction. **f** 'Gold-standard' Fourier shell correlation curves of the lasmiditan–5-HT_{1F}–G_i complex.

a

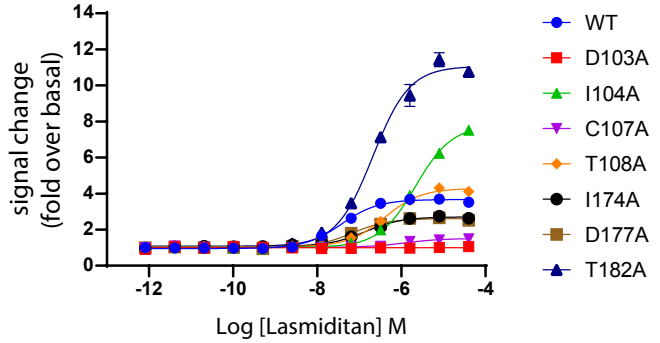

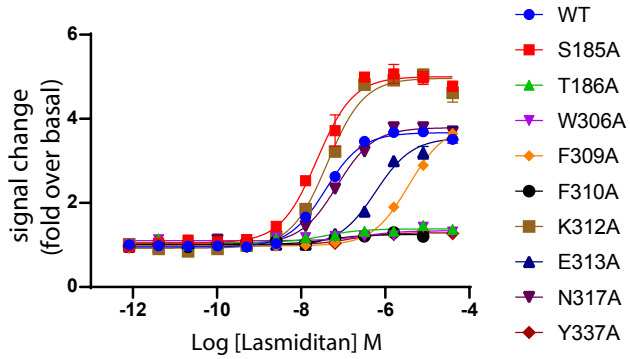

b

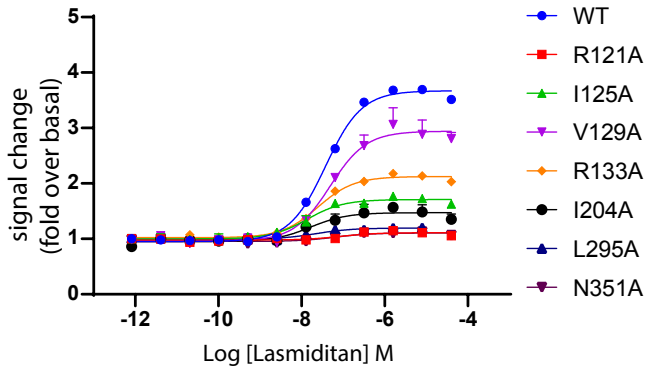

c

Const.	pEC50	ΔpEC50
R121A	7.07 ± 0.31	-0.35
I125A	7.86 ± 0.13	0.44
V129A	7.31 ± 0.10	-0.11
R133A	7.61 ± 0.06	0.19
I204A	7.78 ± 0.29	0.36
R287A	7.15 ± 0.05	-0.27
L295A	7.65 ± 0.15	0.23
N351A	7.20 ± 0.34	-0.22
ECL2(1A)	< 4.0	< -3.42
ECL2(1B)	< 4.0	< -3.42
ECL2(1D)	< 4.0	< -3.42
ECL2(1E)	< 4.0	< -3.42

d

Const.	pEC50	ΔpEC50
WT	7.42 ± 0.03	0
D103A	< 4.0	< -3.42
I104A	5.66 ± 0.01	-1.76
C107A	5.91 ± 0.12	-1.5
T108A	6.40 ± 0.03	-1.02
T182A	6.67 ± 0.04	-0.74
S185A	7.62 ± 0.06	0.2
T186A	7.43 ± 0.29	0.01
W306A	< 4.0	< -3.42
F309A	5.44 ± 0.02	-1.98
F310A	< 4.0	< -3.42
K312A	7.38 ± 0.05	-0.04
E313A	6.23 ± 0.06	-1.19
N317A	7.15 ± 0.03	-0.27
Y337A	< 4.0	< -3.42
I174A	6.86 ± 0.04	-0.56
D177A	7.17 ± 0.04	-0.25

Supplementary information, Fig. S2 Mutagenesis data of lasmiditan-mediated 5-HT$_{1F}$ activation by NanoBiT Gi protein recruitment assay. a Dose response curves of mutations on ligand-binding pocket. **b** Dose response curves of mutations on G protein interaction interface. **c** pEC$_{50}$ of mutations on G protein interaction interface and ECL2 chimeraic receptors. **d** pEC$_{50}$ of mutations on ligand-binding pocket. Data are mean ± s.e.m. from at least three independent experiments performed in technical triplicate.

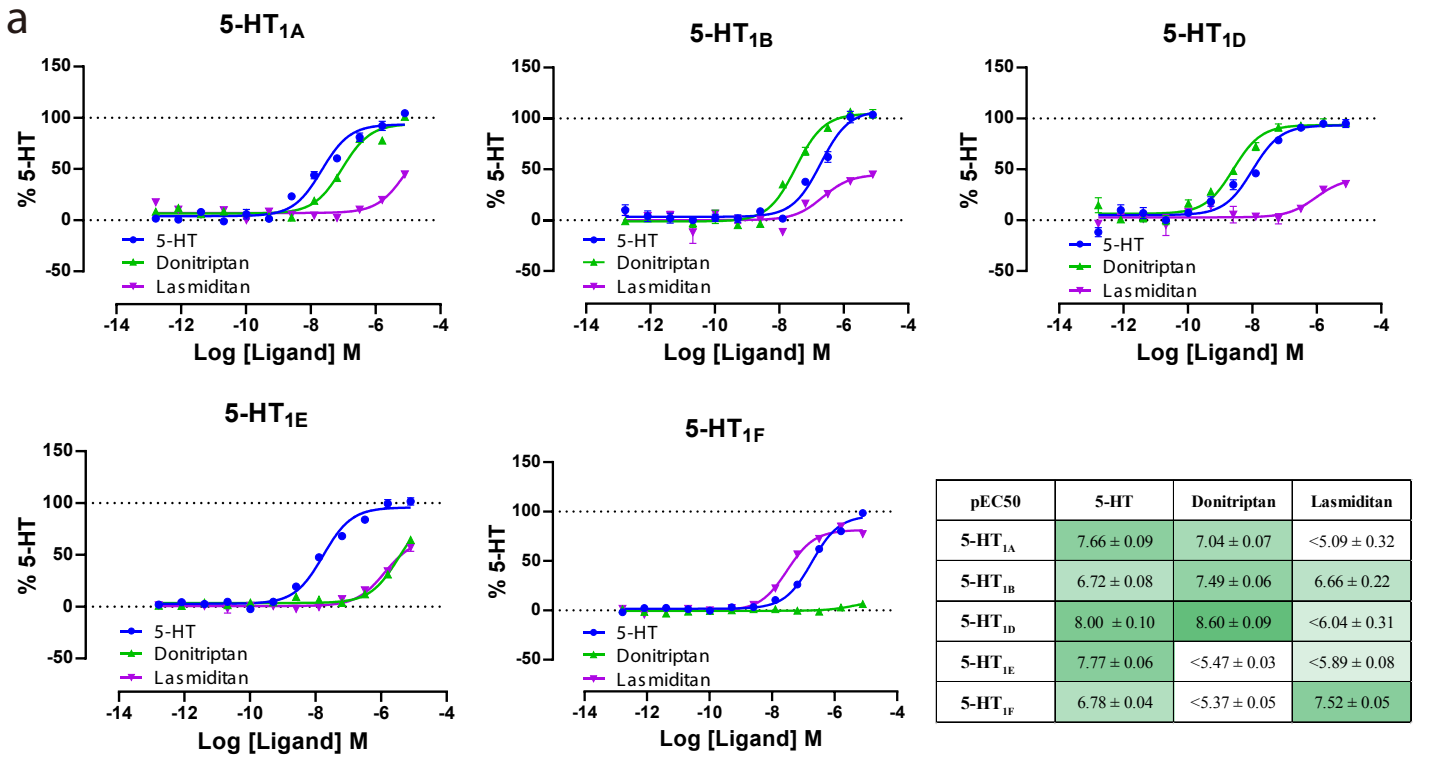

pEC50	5-HT	Donitriptan	Lasmiditan
5-HT_{1A}	7.66 ± 0.09	7.04 ± 0.07	<5.09 ± 0.32
5-HT_{1B}	6.72 ± 0.08	7.49 ± 0.06	6.66 ± 0.22
5-HT_{1D}	8.00 ± 0.10	8.60 ± 0.09	<6.04 ± 0.31
5-HT_{1E}	7.77 ± 0.06	<5.47 ± 0.03	<5.89 ± 0.08
5-HT_{1F}	6.78 ± 0.04	<5.37 ± 0.05	7.52 ± 0.05

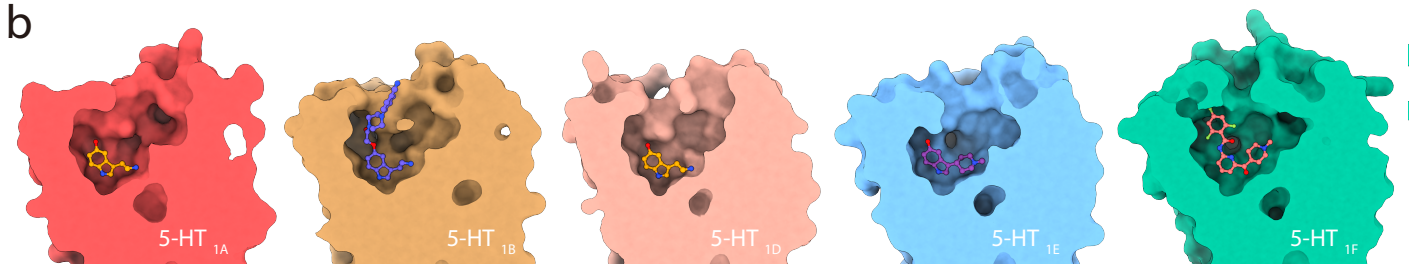

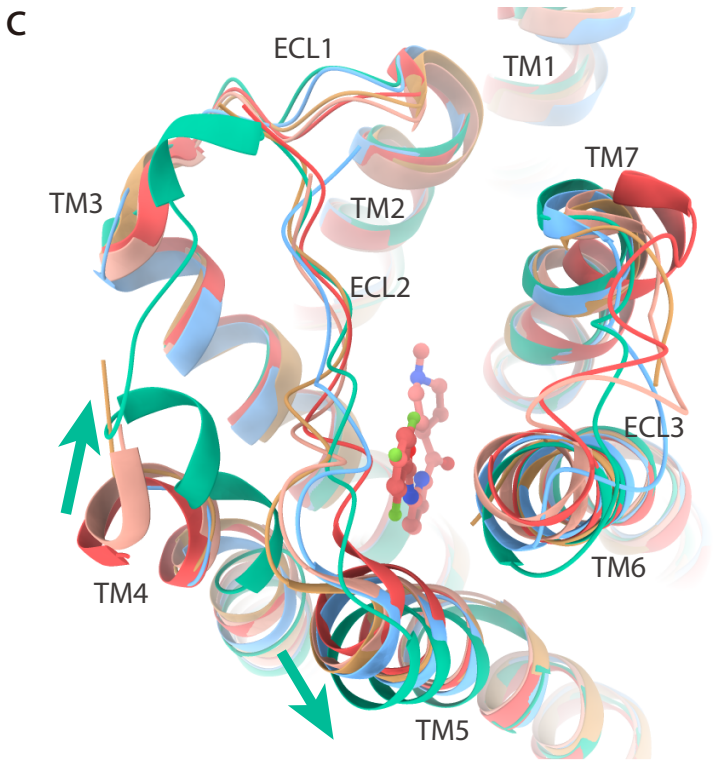

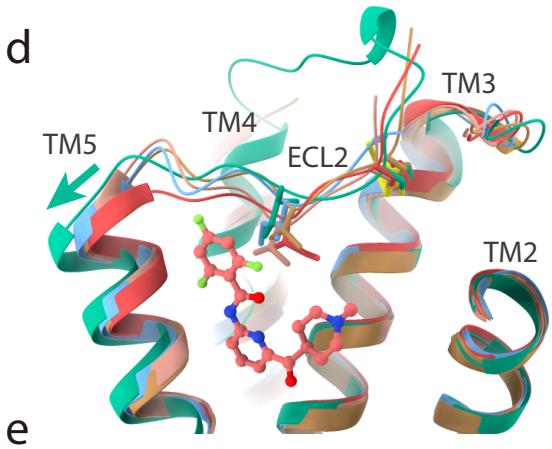

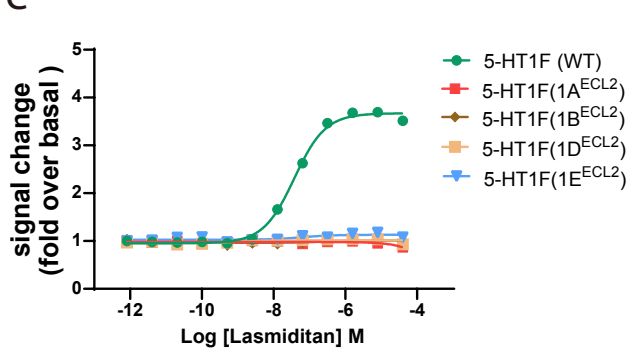

Supplementary information, Fig. S3 Selectivity of lasmiditan. a Dose response curves and pEC50 of 5-HT, donitriptan, and lasmiditan induced activation of 5-HT_{1A}, 5-HT_{1B}, 5-HT_{1D}, 5-HT_{1E} and 5-HT_{1F}. **b** Comparison of the ligand-binding pocket among the structures of $G_{i/o}$-coupled 5-HT_{1A} (red, PDB code: 7E2Y), 5-HT_{1B} (tan, PDB code: 6G79), 5-HT_{1D} (yellow, PDB code: 7E32), 5-HT_{1E} (blue, PDB code: 7E33) and 5-HT_{1F} (green). **c, d** Comparison of TM4–TM5–ECL2 region among 5-HT_1 sub-family receptors. **c**, extracellular view; **d**, side view. **e** The replacement of ECL2 of 5-HT_{1F} with other 5-HT_1 receptors affects the lasmiditan-mediated activation. Data are mean ± s.e.m. from at least three independent experiments performed in technical triplicate.

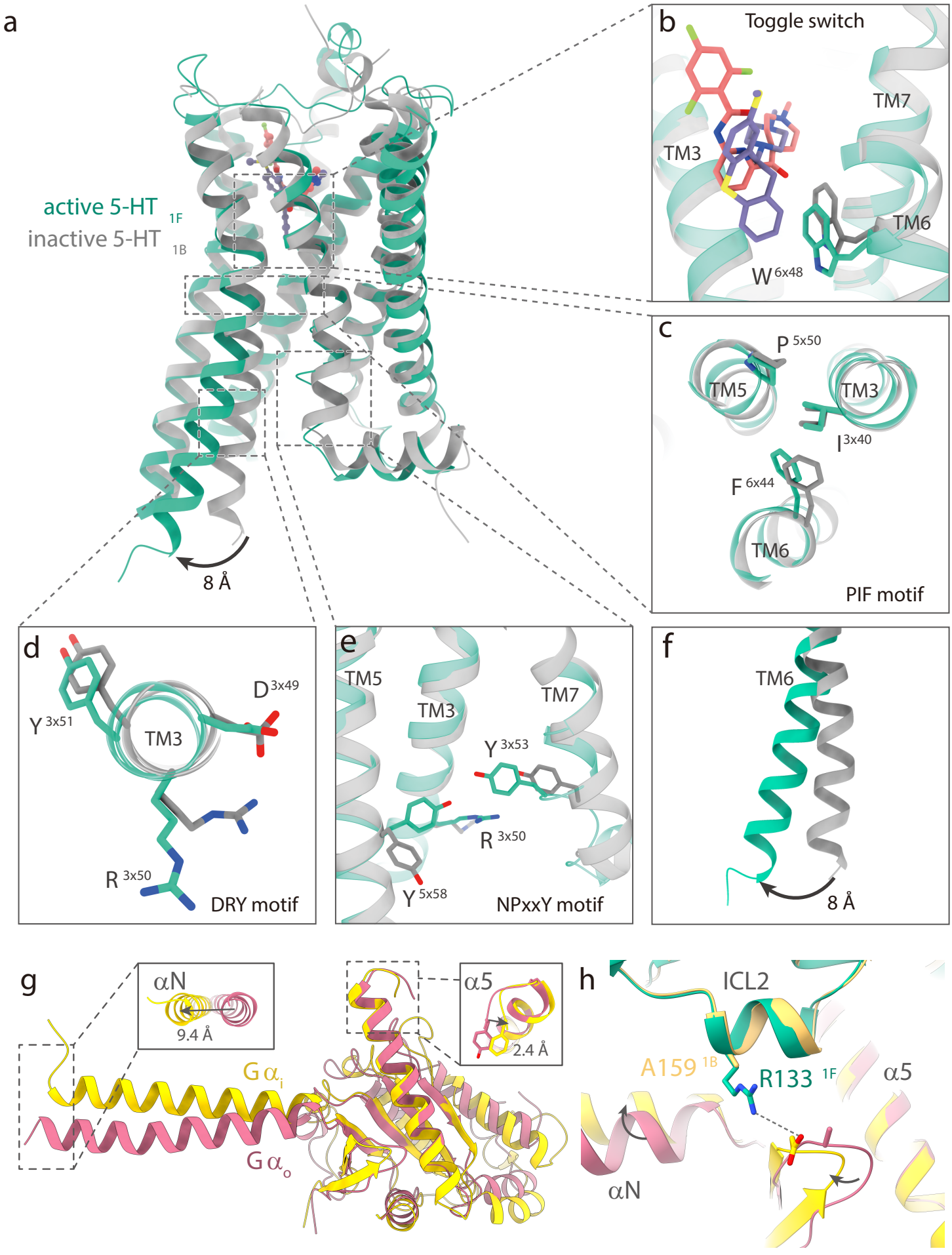
a
active 5-HT 1F
inactive 5-HT 1B
8 Å
b
Toggle switch
TM7
TM3
TM6
W 6x48
c
P 5x50
TM5
TM3
I 3x40
F 6x44
TM6
PIF motif
d
D 3x49
Y 3x51
TM3
R 3x50
DRY motif
e
TM5
TM3
TM7
Y 3x53
R 3x50
Y 5x58
NPxxY motif
f
TM6
8 Å
g
αN
9.4 Å
α5
2.4 Å
Gαi
Gαo
h
ICL2
A159 1B
R133 1F
α5
αN

Supplementary information, Fig. S4 Lasmiditan-induced activation of 5-HT$_{1F}$. a Structural superposition of active 5-HT$_{1F}$ and inactive 5-HT$_{1B}$ (PDB code: 5v54) complexes. **b-e** Residue rearrangement of Toggle switch (**b**), PIF motif (**c**), DRY motif (**d**), and NPxxY motif (**e**). **f** The outwad movement of intracellular end of TM6. **g** Comparison of the 5-HT$_{1F}$-bound Gα_i conformation and 5-HT$_{1B}$-bound Gα_o conformation. The left arrow indicates the movement of αN helix in Gα_i structure relative to Gα_o structure. The right arrow indicates the movement of the last amino acid in the Gα α5 helix in Gα_i structure relative to Gα_o structure. **h** Comparison of ICL2–G protein interactions in the 5-HT$_{1F}$–G$_i$ and 5-HT$_{1B}$–mG$_o$ structures.